PROGRESS IN PHOTOVOLTAICS: RESEARCH AND APPLICATIONS
Prog. Photovolt: Res. Appl. (2012)
Published online in Wiley Online Library (wileyonlinelibrary.com). DOI: 10.1002/pip.2186

RESEARCH ARTICLE

Reflection distributions of textured monocrystalline silicon: implications for silicon solar cells

Simeon C. Baker-Finch[1]* and Keith R. McIntosh[2]

[1] College of Engineering and Computer Science, Australian National University, Canberra, ACT 0200, Australia
[2] PV Lighthouse, Coledale, NSW 2515, Australia

ABSTRACT

A common misconception is that alkaline textured silicon solar cell surfaces are characterised by features that are pyramidal and bounded by {111} planes. In preference to the typical approach of observing scanning electron microscope images, we analyse reflection distributions from various pyramidal textures and find that {111} faceted pyramids are a poor approximation to the features on such surfaces. We conclude that features are hillocks, with an octagonal base. Furthermore, the characteristic base angle of the texture depends on the etchant and is closer to 50–52° than the commonly accepted value of 54.74°. Analyses of antireflection, light trapping, photogeneration and surface recombination properties of textured surfaces should take this feature morphology into account. The base angle has a strong influence on the hemispherical reflectance of the textured surface, with higher angles resulting in reduced reflectance. The influence of this reflection enhancement upon device performance is smallest when an optimised antireflection coating is applied; compared with an array of {111} faceted pyramids, a hillock morphology with 50° base angle results in a 0.2% reduction in photogenerated current in a typical cell. Additionally, as base angle is reduced, an encapsulant of increasingly higher refractive index is required to drive internal reflection at the air–glass interface of light initially reflected from the cell surface. The development of texturing processes resulting in higher base angles is encouraged. Copyright © 2012 John Wiley & Sons, Ltd.

KEYWORDS

texture; reflection distribution; optics; ray tracing; antireflection coating

***Correspondence**
Simeon C. Baker-Finch, College of Engineering and Computer Science, Australian National University, Canberra, ACT 0200, Australia.
E-mail: simeon.baker-finch@anu.edu.au

Received 21 October 2011; Revised 13 December 2011; Accepted 10 February 2012

1. INTRODUCTION

The sunward surface of a silicon solar cell is almost always textured. When the surface is rough, rather than planar, light is more effectively coupled into, and retained inside, the active region of such a device. Monocrystalline silicon wafers are most commonly processed in an alkaline texturing solution that is intended to produce a random array of upright pyramids on the etched surface. It is the anisotropic nature of such an etchant (where the etch rate in the <100> direction is several times greater than that in the <111> direction) that drives the formation of a repeated pyramidal or hillock feature. Many and varied etchants have been investigated, including aqueous solutions of NaOH [1,2], Na_2CO_3 [3–5], KOH [6] and TMAH [7,8]; the success or otherwise of the process tends to depend on temperature and composition of the solution (the addition of isopropyl alcohol (IPA) is often critical) as well as the pre-etch properties of the silicon surface. The final morphology of the features has various implications for the performance of silicon solar cells; front-surface reflectance, light trapping capacity, module performance and surface recombination may all be affected.

Typically, scanning electron microscope images of the variety depicted in Figure 1 are used to assess textured silicon (see, e.g. [2,9]). Such images are usually provided as evidence that the texture consists of ideal {111} faceted upright pyramids. More careful examination of the features usually suggests otherwise [10,11]. Indeed, in fields of micromachining, texture features have been studied extensively [10–14]. However, relatively few conclusions have been transferred into the analysis of surface texture in silicon solar cell applications. What is generally, and often errantly, assumed to be a texture consisting of upright tetrahedral features bounded by {111} planes (i.e. square-based pyramids, as shown at the left in Figure 2(a)) is probably an assortment of so-called 'hillocks' [10,13,14]. Depending on the etching conditions, the hillocks range from near-perfect upright pyramids with some slight bowing of the facets or bevelling of edges [12] to features with distinctly octagonal (rather

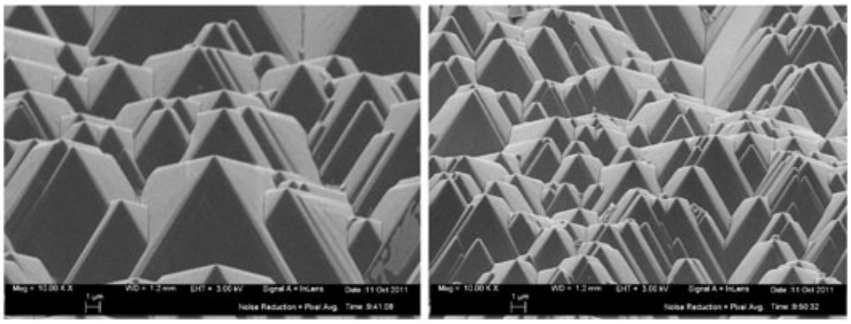

Figure 1. Scanning electron microscope images of silicon textured in alkaline solution, taken at 45° tilt. The sample at the left is textured in a TMAH solution, and the sample at the right is textured in a KOH solution. The images depict the samples used in the experimental work outlined in Section 3.

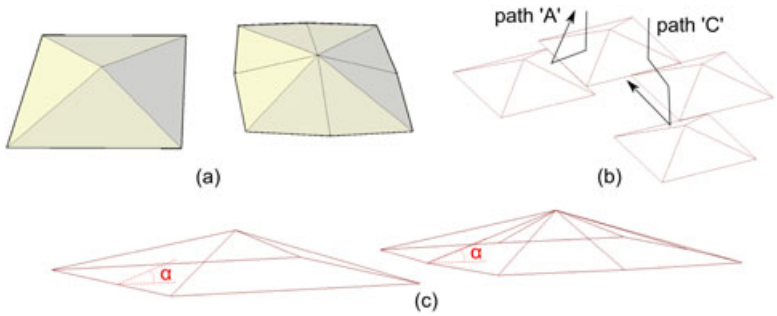

Figure 2. (a) A representation of a near {111} faceted pyramid (left) and a hillock, with octagonal base (right). (b) Dominant paths of reflection at pyramidal texture, after [20]. (c) The characteristic base angle α of a pyramid or hillock is defined as the inclination of the facets with respect to the <100> oriented base.

than quadrilateral) bases [10] of the kind illustrated at the right in Figure 2(a). The precise mechanism for the development of such hillocks remains contentious; two likely contributors are as follows: (i) the exposure of a convex corner of the growing feature results in the etching of higher index 'bevelling' planes that eventually intersect to form a stable bowed facet; and (ii) the formation of kinks or ledges (terrace-like structures—see the bottom right corner of the leftmost image in Figure 1 for an example) on the pyramid facet as etching proceeds [10–14].

Additionally, the angle between the macroscopic surface and each plane of the hillock or pyramid (defined in Figure 2(c) and referred to hereafter as the base angle α) is usually less than the angle that would be observed for ideal {111} bounded pyramids (i.e. $\arctan\sqrt{2} = 54.74°$). Typical industrial cells may have α between 49° and 53° [15,16], but certain etchants may result in 'flatter' features, with α as low as 45° [13]. As we discuss in detail in the following text, α is particularly critical to the modelling and performance of the textured solar cell surface.

Texture morphology has a decisive impact on the antireflective capacity of the sunward surface of the cell, as well as implications in antireflection coating (ARC) optimisation and light trapping. Furthermore, α determines the extent to which reflected light is given a second chance to be absorbed by the cell when encapsulated (following internal reflection at the glass–air boundary). As well, it is likely that minor variations in morphology influence surface recombination and passivation. Given that the texture morphology evolves as the composition of an etch bath changes, a method for characterisation of the evolving morphology is a critical precursor to precise process control. One such method is developed in this paper. Furthermore, a more accurate geometric model of the surface, derived from the application of this method, offers a guide for the improvement of current optical models of the textured silicon surface.

The analysis of the reflection distribution of textured silicon has been suggested as a means of assessing the ability of the surface morphology to contribute positively to the efficiency of a completed solar cell device [15,17–19]. Usually, the measurement apparatus includes a laser aligned to the sample normal and a photosensitive screen [15] or an array of photodiodes [16] for capturing the reflected radiation. The approach of Fornies *et al*. [15] is to determine a figure of merit that represents the proportion of flat areas on the sample, where texturing has not occurred. This figure of merit is simply equal to the ratio of the light reflected along 'A' paths (Figure 2(b)) to the light reflected normal to the sample. The approach is well suited to inline assessment of texture quality, but further analysis of the reflection distribution offers an improved understanding of the texture morphology.

DOI: 10.1002/pip

In this work, we present a methodology for the quantitative measurement of the reflection distribution of textured silicon. In particular, we employ a spectrophotometer with an angular reflectance accessory to determine such distributions for silicon samples featuring either a regular array of inverted pyramids having {111} facets or a random array of pyramidal or near pyramidal features. The measurement is sufficiently sensitive to detect the reflectance from both 'A' and 'C' paths (Figure 2(b) or [20] for more detail) from inverted pyramid texture. Critically, we find this technique to provide direct access to the morphology of the texture features; unlike the scanning electron microscope image analysis approach, the assessment of optical reflection distributions is sensitive to the presence of hillocks and to lower-than-ideal values of α.

Reflection distributions emerging from random texture suggest that a commonly used geometric approximation (namely that texture features are tetrahedral, with {111} facets) is flawed in two ways: (i) the angle between the feature base and facets is significantly less than expected; and (ii) the base of each feature is not square, but octagonal, so that there are eight (rather than four) facets of each feature, and these features have a combination of orientations (and that these orientations are higher index planes, not {111}).

The implications of these findings for the optical analysis of silicon solar cells are manifold: (i) the antireflection and light trapping action of the texture is determined by its precise morphology; (ii) the capture of reflected light in the module in which the cell is encapsulated depends on the angular distribution of reflection; and (iii) flatter features may potentially be better passivated than sharper ones. The accurate characterisation of textured silicon tends to depend on a reasonable approximation of the front surface texture geometry.

2. VARIABLE ANGLE SPECTROPHOTOMETRY FOR ASSESSMENT OF SILICON SOLAR CELL TEXTURE

2.1. Theory and experimental apparatus

Variable angle spectrophotometry is a technique that typically complements or replaces spectroscopic ellipsometry as a means for determining the thickness and refractive index of thin films [21]. The experimental apparatus, specifically a spectrophotometer equipped with motorised stages (goniometers), allows sample and detector angles to be varied with a high degree of accuracy [22]. Variable sample and detector angles render the apparatus capable of a broad range of measurements including those of angular resolved scattering and bidirectional reflectance/transmittance distribution functions.

In this work, we employed a Perkin Elmer Lambda 1050 spectrophotometer along with an Absolute Reflectance/Transmittance Analyser accessory from OMT Solutions (Eindhoven, The Netherlands) [21]. The experimental layout is illustrated in Figure 3(a). An integrating sphere of 65-mm diameter served as detector of the normally incident, polarised light that is reflected from the sample with angle $\theta_r \pm \omega_d$ to the macroscopic normal of the sample surface. For the measurements undertaken in this work, the detector opening width $\omega_d = 0.25^\circ$, meaning that measurements of reflectance R as a function of θ_r represent the integrated reflectance in a 0.5° wide slice of the reflection distribution function. As illustrated in the isometric representation of the apparatus in Figure 3(b), the zenith angle ϕ_r was adjusted by rotation of the sample about the incoming beam path; we define $\phi_r = 0$ when the <110> flat, the incoming beam and the detector are coplanar. The detector opening corresponds to $\pm 7.5^\circ$ resolution in ϕ_r. In total, the detector opening subtends a solid angle of ~0.002 steradians of the reflectance sphere.

Note that the incident beam is not collimated; rather, as shown in Figure 3(c), it is focused so as to obtain an image of the monochromators slit on the sample surface. A wider beam (in which the energy is distributed over approximately 10°) is hence found at the entrance to the integrating sphere. As is shown in Figure 3(c) and (d), the non-collimation of the beam at the sample results in a broader beam divergence at the detector. We used an inverted pyramid textured silicon wafer as a means or correcting for this divergence; a technique for doing so is described in the following text.

Rays normally incident to a textured surface are typically reflected along a number of discrete paths [20]. The proportion of the incident radiation reflected at a particular θ_r and ϕ_r depends on the proportion of rays reflected along a certain path, as well as the reflectance of that path. With a collimated beam, we would therefore expect to measure distinct delta function peaks in the reflection distribution functions at pairs (θ_j, ϕ_j), where j represents one particular path (A thru G in [20]).

The sensitivity of our measurements (~0.01% of the incident radiation) limits us to the observation of paths having at least moderate reflectance and, most importantly, a high 'path fraction' (usually paths A and C). We measured the reflection distribution function with incident radiation having a 270-nm wavelength. Advantageously, this wavelength is well below the texture feature size, thus rendering diffractive effects negligible (perhaps with the exception of diffraction at sharp peaks or troughs). As evidenced in the following text, the reflectance signal at this wavelength was sufficiently high that noise did not adversely impact upon our measurements.

2.2. Reflection distribution from regular inverted pyramids

We probed a sample having known surface morphology, namely a regular array of inverted pyramids, to validate the experimental setup. In the following, we find close agreement between experiment and a reflection distribution determined by ray tracing. Additionally, the measurement of a known structure allows us to quantify the impacts of the non-collimation of the incident beam.

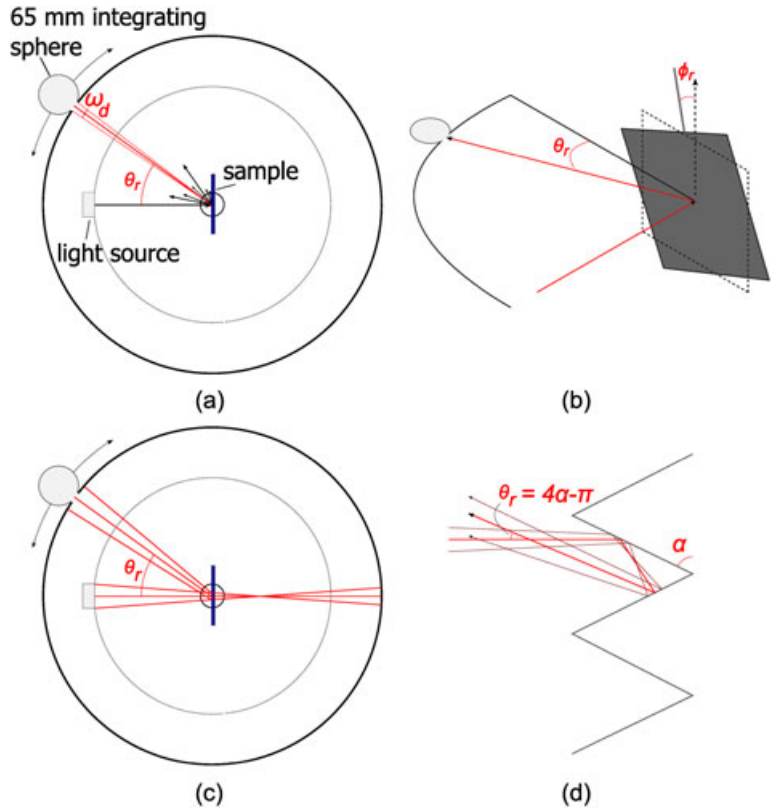

Figure 3. (a) The Absolute Reflectance/Transmittance Analyser apparatus consists of light source, sample and integrating sphere detector; the detector is located at some angle θ_r with respect to the beam of the light source. (b) As shown in this isometric representation, the zenith angle ϕ_r is controlled by rotating the sample (shown in grey) about the axis of the incoming beam. (c) The incoming beam is focused, rather than collimated, resulting in a broad reflected beam at the detector. (d) The source of the beam broadening is illustrated when reflection occurs along path A; a non-collimated incoming beam results in a non-collimated reflected beam.

A bare silicon sample was textured with a regular array of inverted pyramids via photolithographic masking and etching in 25% TMAH at 85 °C. The process of masking and anisotropic etching resulted in pyramids having very nearly perfect {111} facets and a characteristic angle $\alpha = 54.74°$. The sample was first placed at the central axis of the experimental apparatus with the pyramids aligned such that the 'path A' reflection was in the plane of the detector rotation ($\phi_r = 0$). Rather than a single reflection peak at $\theta_r = 4\arctan\sqrt{2} - \pi = 38.94°$, a broad peak of reflectance was measured, as shown in Figure 4(a). The distribution of the reflected light over a range of angles is attributable to the divergence of the reflected beam mentioned previously and illustrated in Figure 3(d).

In Figure 4(b), a similar but smaller peak is found in the scan for $\phi_r = 45°$; this peak corresponds in both location and magnitude to path 'C'. At intermediate values of ϕ_r, smaller peaks were measured. In an ideal case, no such peaks would exist; we suspect that the limited resolution of the experimental apparatus in the ϕ_r axis was the source of these peaks. Despite these minor aberrations, it is apparent that the experimental apparatus is well suited to measuring the reflection distribution function from a textured silicon sample. The experimental data shown here closely match values determined via ray tracing analysis. Note in particular that the integral of the broad reflectance peak in Figure 4(a) matches that of the ideal delta function within 0.5%.

One may delineate the impact of the beam spreading in a function representing the reflection distribution function. Note that the integral of the reflectance peak for $\phi_r = 0$ is given by

$$\int_0^{\pi/2} R(\theta', 0)\,\mathrm{d}\theta' = f_A R_A/4, \tag{1}$$

where f_A and R_A are the path proportion and reflectance along the path, as described in [20]. We further define the distribution function g such that

$$R(\theta, 0) = g(\theta - \theta_0) f_A R_A/4, \tag{2}$$

where θ_0 is the angle at which all light would be reflected without beam spreading (θ_0 depends on the characteristic angle of the texture with $\alpha = (\theta + \pi)/4$). Intuitively, $\int g\,\mathrm{d}\theta = 1$. We apply g in Section 3.2 to derive reflection distributions accounting for beam divergence (illustrated in Figures 5(a) and 6(a)) and to calculate possible distributions of

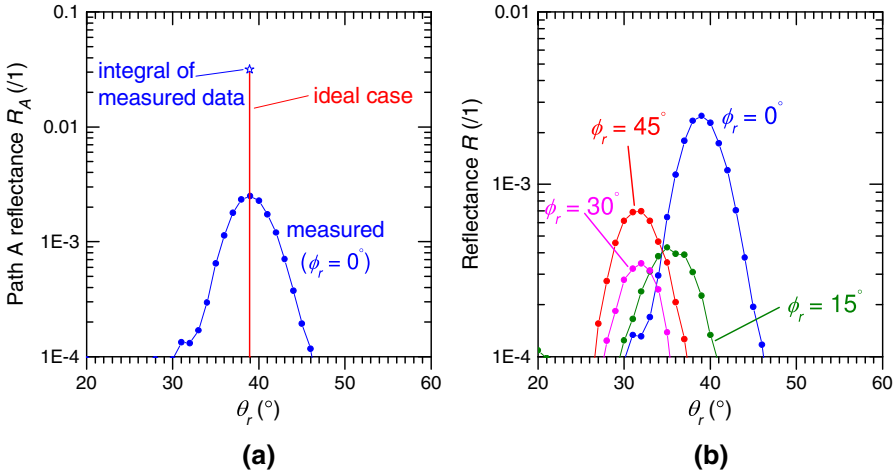

Figure 4. Measured reflection distribution from a silicon surface textured with a regular array of inverted pyramids. In (a), the integral of the reflectance beneath the broad measured peak matches closely the integral of the delta function determined by ray tracing. In (b), the reflectance for a range of values of ϕ_r is shown; the majority of reflection is, as expected, in the $\phi_r = 0°$ and 45° directions. Note that the data would more accurately be represented as a histogram, with bin width 0.5° on the θ_r axis.

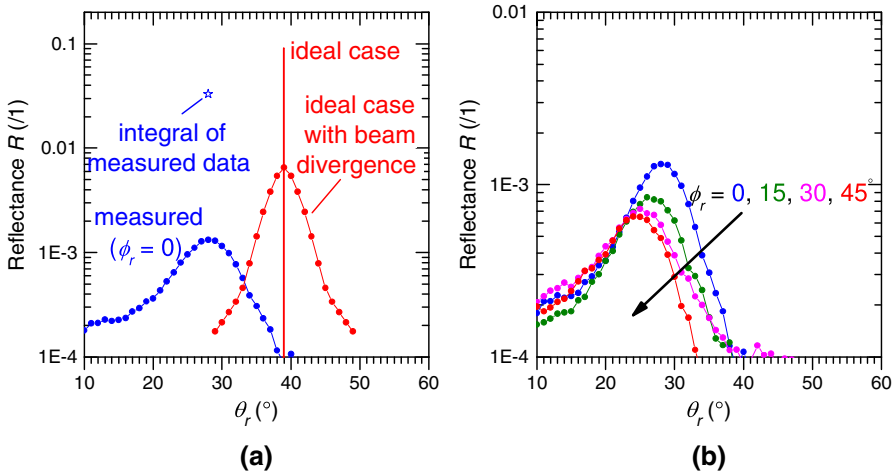

Figure 5. Measured reflection distribution from a silicon surface textured in a TMAH solution. In (a), the measured $\phi_r = 0°$ reflection distribution is compared with the delta function reflectance expected from a random array of {111} faceted pyramids. Also plotted is the representation of that delta function when beam divergence is taken into account. In (b), the experimental reflection distribution is shown for a range of ϕ_r. For θ_r beyond 60°, reflectance values below the sensitivity limit of the instrument ($\sim 1 \times 10^{-4}$) are observed.

characteristic base angles on surfaces featuring random upright pyramid or hillock textures (Section 3.5).

3. ASSESSMENT OF RANDOM TEXTURE WITH VARIABLE ANGLE SPECTROPHOTOMETRY

3.1. Approach

Having validated the experimental apparatus, we set about comparing reflection distributions determined experimentally on random texture with the distribution predicted by ray tracing of the ideal tetrahedral pyramid morphology. Below, we compare the experimental data with more complex ray traced reflection distributions; these distributions are calculated by assuming either (i) surface features are near {111} faceted upright pyramids, with $\alpha = 50°$ or (ii) features are hillocks, having near {567} facets [10]. That the measured data for a pair of textured samples is not consistent with the reflection distribution expected from an array of {111} faceted upright pyramids suggests that a reassessment of surface morphology is in order.

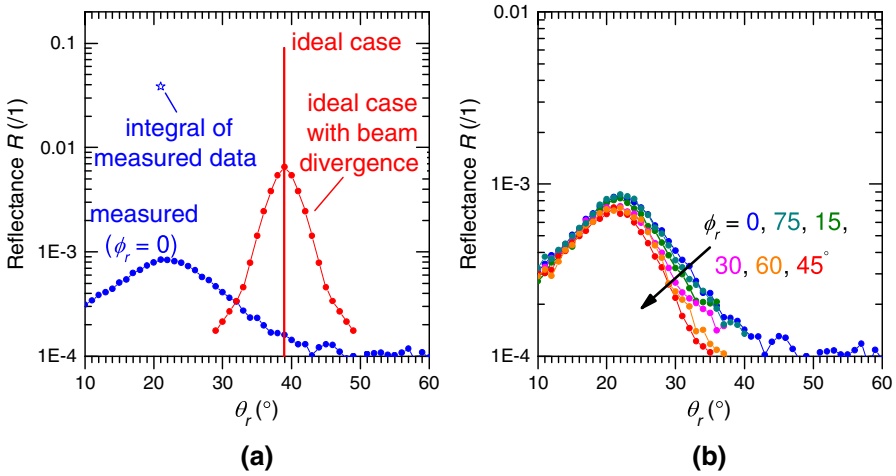

Figure 6. Measured reflection distribution from a silicon surface textured in a KOH solution. Details are the same as for Figure 5.

3.2. Measured reflection distribution functions

Bare silicon was textured in an alkaline solution of tetramethylammonium hydroxide (TMAH, 25 wt%), H_2O and IPA (volume ratio 6:1:1), with additional dissolved silicon, for 60 min at a temperature of 85 °C. A second sample was acquired from a large manufacturer of silicon solar cells; presumably this sample was textured in an aqueous KOH solution with additional surfactant (IPA or similar). We applied the technique described previously to determine the reflection distribution function of each sample and plot the results in Figures 5 and 6.

In Figures 5(a) and 6(a), we plot the reflection distributions measured about $\phi_r = 0$ and compare them with the ideal delta function (at $\theta_r = 38.9°$) that was determined via ray tracing simulations of a random array of {111} faceted upright pyramids. We also re-plot the delta function as the broad peak that we expect to result from the reflection of the divergent beam. Neither textured sample exhibits the reflection distribution function that one would expect from a sample textured with {111} faceted upright pyramids. We note three key discrepancies. The location, breadth and integral of the measured peaks do not match modelled equivalents.

Firstly, we observe that the peak of the $\phi_r = 0$ reflectance peak is located at either $\theta_r = 28°$ or $\theta_r = 22°$, rather than at $\theta_r = 38.9°$. The peak location is a sensitive indicator of the dominant characteristic base angles α of the texture features, and the measured distributions indicate that the typical features are 'flatter' ($\alpha \approx 52°$ or $\alpha \approx 50°$) than what would be expected from {111} facets on an originally <100> surface ($\alpha \approx 54.74°$).

Secondly, we note that the peak in experimental reflection distribution is broader than that expected from simulation; this phenomenon is particularly noticeable in Figure 6 (a), where the sample is etched in a KOH solution. This implies that the texture features a distribution of α values. Likely, values are determined in Section 3.5.

Thirdly, we note that the integral of the measured distributions (representing the total reflectance in the $\phi_r = 0$ region) is 36–42% of the value determined by ray tracing. This observation, when combined with the results of measurements at different values of ϕ_r, is a strong indicator that the surface texture on the experimental samples exhibits hillock rather than pyramidal features.

Experimentally determined reflection distributions for a range of ϕ_r are plotted in Figures 5(b) and 6(b). We observe significant reflectance at $\phi_r = 15°$, 30°, 45° (and at $\phi_r = 60°$, 75° for the KOH etched sample). In the case of the TMAH etched sample, we observe a peak of decreasing magnitude shifting to lower values of θ_r as ϕ_r increases from 0° to 45°. On the other hand, the reflection distribution from the KOH textured sample exhibits yet broader peaks, and little dependence on ϕ_r is observed. In an attempt to better understand the phenomena behind the measured reflection distributions, we undertook to assess various texture morphologies via ray tracing. In particular, as described in the following text, we derived the reflectance patterns that would be observed experimentally were the texture to consist of well-defined features of various morphologies.

3.3. Reflection distribution functions determined by ray tracing

We applied geometrical ray tracing of the sort that is commonly used in photovoltaics and is described in detail elsewhere [20] in order to determine the reflection distribution functions for a range of surface morphologies computationally. As shown in Figure 7, we calculated reflection distributions for the following: (a) {111} faceted upright pyramids ($\alpha = 54.74°$) and (b) near {111} faceted pyramids with $\alpha = 50°$. Additionally, we calculated the more complex distributions from the following: (c) near {567} faceted hillocks with $\alpha = 54.74°$ and (d) near {567} faceted hillocks with $\alpha = 50°$.

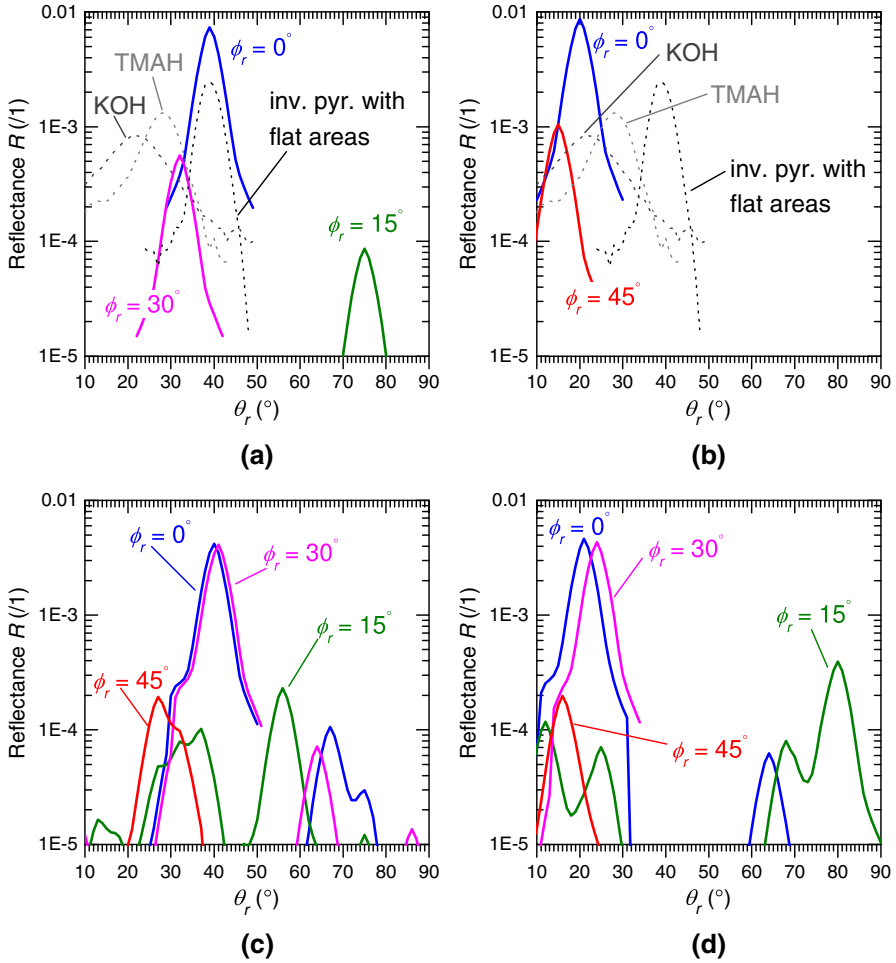

Figure 7. Reflection distributions as calculated by ray tracing for: (a) {111} faceted upright pyramids; (b) near {111} faceted pyramids with $\alpha = 50°$; (c) near {567} faceted hillocks with $\alpha = 54.74°$; (d) near {567} faceted hillocks with $\alpha = 50°$. Note that the beam divergence effect described in the text is accounted for by spreading of the ray traced delta functions of reflectance to nearby θ_r (via convolution with the function *g*). In (a) and (b), experimental reflection distributions for the various samples at $\phi_r = 0°$ are included for reference.

To mimic the reflection distribution that would be measured by our experimental apparatus, the results illustrated in Figure 7 were determined by the convolution of the spreading function *g* with the distinct peaks (corresponding to discrete reflection paths) that were found by ray tracing. We integrated over the relevant range of ϕ_r for each curve shown in the following text to simulate the impact of the 15° resolution in this dimension.

The reflection distribution from a random array of upright pyramids bounded by {111} facets exhibits a large reflectance peak at $\phi_r = 0$, as shown in Figure 7(a). The peak is several times larger than the one observed for the inverted pyramid textured sample (which has flat areas) and has a location in θ_r space determined by the characteristic angles of the random pyramids—with $\alpha = 54.74°$, the peak is centred at $\theta_r = 38.9°$. As shown in Figure 7(b), for a similar morphology differing only by the reduced α (50° rather than 54.74°), the dominant peak is shifted to $\theta_r = 20°$. In Figure 7(a) and (b), smaller peaks are present at $\phi_r = 15°$, 30° and 45°. Note that we re-plot the experimental data at $\phi_r = 0$ for reference.

A more complex reflection distribution was derived from ray tracing simulations of randomly arranged hillocks. To arrive at the results illustrated in Figure 7(c) and (d), we assumed that the hillocks have an octagonal base, with the intersection between each facet and the initially <100> surface described by a line with a [560] orientation [10]. The position of each neighbouring hillock was simulated in an identical fashion as to the random upright pyramids of [20]. Note the presence of strong peaks in the reflection distribution function for both $\phi_r = 0°$ and $\phi_r = 30°$. The reduction of α from 54.74° (Figure 7(c)) to 50° (Figure 7(d)) shifts the two peaks to the left on the θ_r scale.

We further extended the simulations to a case in which hillock features exhibit a range of values of α. Assuming a uniform distribution of features with $\alpha = 50°$, 51°, 52° or 53°, we calculated the reflection distribution illustrated in Figure 8. Note the comparatively broad peaks representing

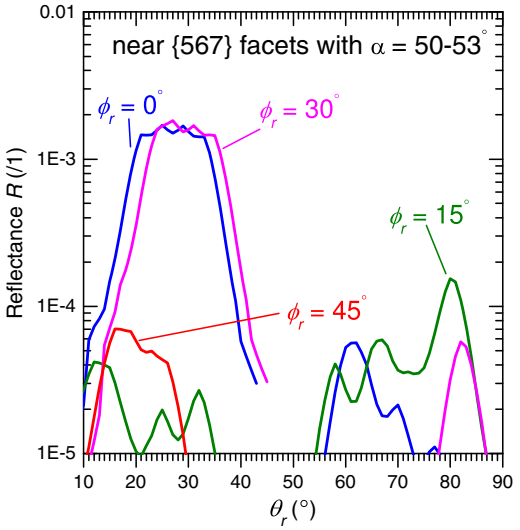

Figure 8. Reflection distribution as calculated by ray tracing for a surface texture consisting of hillocks having α distributed uniformly between 50 and 53°.

the reflectance at $\phi_r = 0°$ and $\phi_r = 30°$. As discussed previously, the impact of a range of α is to broaden such peaks. Although in general, a range of α does not cause other significant changes in the reflection distribution function; in particular, reflection does not move significantly in the ϕ_r axis (at least on the coarse scale used here).

3.4. Comparison of measured and modelled reflection distributions

The comparison of modelled and measured reflection distributions makes it clear that {111} faceted upright pyramids are a poor approximation to the features found on textured silicon of the kind typically used in solar cell manufacture. Certainly, the characteristic angles α of samples are significantly less than 54.74°. Furthermore, that significant reflection is observed in the $\phi_r = 15°$ and 45° ranges (and to a lesser extent at $\phi_r = 30°$) indicates that pyramid facets are imperfect (or, equivalently, that the features are hillocks). We are not able, however, to conclude that the features have near {567} facets (as suggested by Tan *et al.* [10]; note that we do not experimentally observe the small peak at $\theta_r \sim 80°$ in the $\phi_r = 15°$ curve). Instead, we suspect that our measured samples are characterised by octagonal hillocks with a range of facet orientations (some near {111} and some with higher indices).

3.5. Approximating α by assessing the $\phi_r = 0°$ reflection distribution

Assuming that the reflection distribution curves at $\phi_r = 0$ are dominated by path A reflection, it is possible to deduce the likely distribution of values of α on our experimental samples. We assumed a Gaussian distribution of α and note that path A reflectance has $\theta_r = 2\alpha_1 + 2\alpha_2 - \pi$, where α_1 and α_2 are the characteristic angles of two neighbouring pyramids. Adjusting for the magnitude of the integral of the experimental reflection distribution peaks, we calculated the best fits and α distributions shown in Figure 9 (a) and (b). The best fit to the KOH sample required a distribution of α that is broader and shifted to lower angles. We highlight that this problem is overprescribed—various distributions of pyramids provide equally good fits and the Gaussian approximation is no more valid than another population distribution.

The formation of hillock features during alkaline etching of silicon is a complex process discussed in detail elsewhere [10–13]. However, the simple explanation suggested by Green [23] offers some insight into the mechanism behind

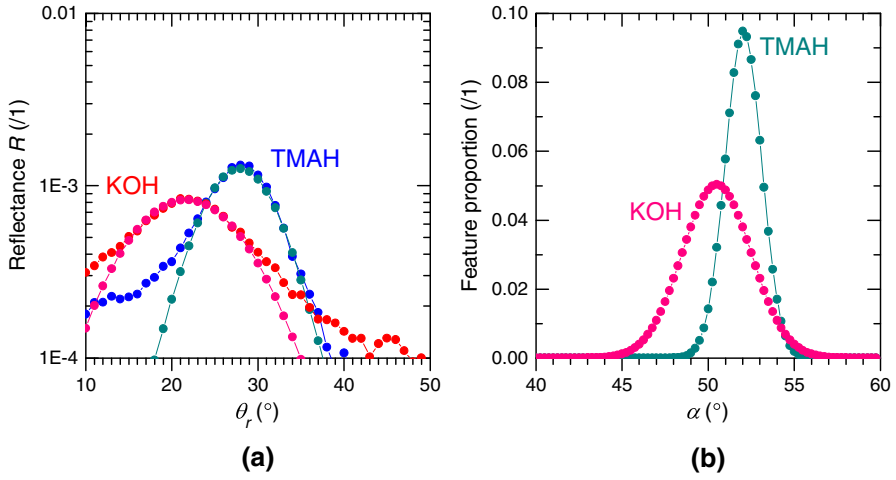

Figure 9. (a) Experimental data and fits to the peaks in reflectance at $\phi_r = 0°$. Fits are calculated by assuming path A reflectance and applying the distribution of base angles shown in (b). Note that both (a) and (b) should strictly be represented as a histogram; (a) has bin width 0.5° on the θ_r axis, and (b) has bin width 1° on the α axis. Gaussian distributions of (b) are centred at 50.5° and 52.1° with standard deviation 2.1° and 4.0° for KOH and TMAH, respectively.

the reduction of α for pyramidal features from the ideal value of 54.74° to the value observed experimentally. In particular, noting that the etch rate of {111} planes is non-zero, Green [23] suggests that α depends on the ratio r of etch rates of {111} and {100} orientations. Rather than Green's $\alpha = \arctan\left(\sqrt{2}\right) - \arctan(r)$, which is inconsistent with his Figure 2(b), we calculate $\alpha = \arctan\left(\sqrt{2}\right) - \arctan\left(\sqrt{2/3}r\right)$. Typical etch rate ratios r vary between 0.005 and 0.2, depending on the etchant, composition (inclusion of IPA or other surfactants), concentration and temperature [2,24–27]. As such, it would be reasonable to expect α to take on values near 54.74° or as low as 45.5°.

Various investigations of surface texture, from ray tracing (e.g. [20,28]) to topographical analysis (e.g. [29]), assume that α takes a value of 54.74°. We suggest that caution be taken with results derived from such analyses. Usually, errors are small, but given the vast range of possible etching processes and resulting surface morphologies, it appears that texture features should be further assessed experimentally (with a focus on determining α).

4. IMPLICATIONS OF IMPERFECT TEXTURE FOR SILICON SOLAR CELLS

Texture morphology has a significant impact on various aspects of silicon solar cell performance and analysis. In general, the industry standard 'random upright pyramid' texture is thought to consist of {111} faceted upright tetrahedral features. This assumption is critical to a range of studies, not limited to those concerning front surface reflectance [20,30], light trapping [28], photogeneration profiles [31–34] and surface passivation [35–39]. We discuss the most important implications of our findings in the following text.

Shown in Figure 10(a) are modelled reflectance curves for a range of texture morphologies. A surface featuring hillocks (perhaps with facets of near {567} orientation but probably having a range of higher index facets) is more reflective than a surface having {111} faceted pyramidal features. More notably, lower values of α result in higher hemispherical reflectance. The hemispherical reflectance dispersion of both KOH and TMAH textured samples is illustrated in Figure 10(b). The experimental reflectance curves are most similar to those expected from samples having near {567} facets and $\alpha = 50°$. However, all simulated curves exhibit lower reflectance than our measurements. We highlight in the following text that the addition of an optimised thin ARC can reduce the relative disadvantage of the hillocks in comparison with {111} faceted pyramids.

Importantly, the front surface morphology determines the optimal thickness and refractive index of the solar cell ARC. Following the optimisation procedure introduced in our previous work [20], for a 200-μm thick cell, we arrive at the results outlined in Table I. The optimal thickness of a SiN_x ARC beneath an encapsulant of ethylene vinyl acetate varies between 74 and 78 nm depending on the facets and α that define the features. Note that with an optimised ARC, the generation current J_g is nearly independent of texture morphology—a 0.2% reduction of J_g is calculated when the texture consists of near {567} faceted hillocks with

Table I. Optimal SiN_x thickness and resulting photogenerated current in cells of 200-μm thickness beneath a range of surface textures.

Morphology	Optimal SiN_x thickness (nm)	J_g (mA cm^{-2})
Pyramid; {111} faceted; $\alpha = 54.74°$	73.6	41.60
Pyramid; near {111}; $\alpha = 50°$	76.2	41.55
Hillock; near {567}; $\alpha = 54.74°$	74.5	41.56
Hillock; near {567}; $\alpha = 50°$	77.7	41.50

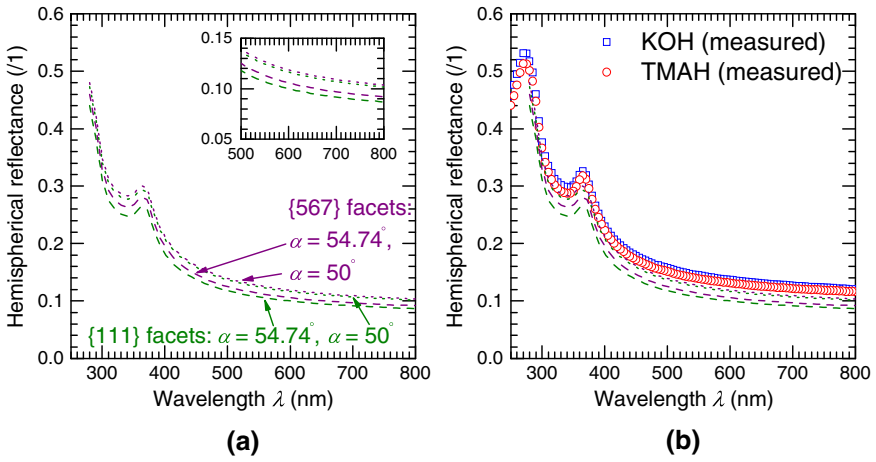

Figure 10. (a) Hemispherical reflectance of bare Si in air, calculated for pyramidal and hillock features with $\alpha = 50°$ or $\alpha = 54.74°$. (b) Comparison of experimental reflectance data with the calculated curves.

$\alpha = 50°$ rather than ideal {111} faceted pyramids. Indeed, with a SiN_x ARC of any thickness between 70 and 80 nm, a maximum of 0.3% deviation in J_g due to morphology is computed. Although low α, hillocks exhibit significantly higher reflectance on bare Si, any negative impact on solar cell performance can be reduced with an appropriate ARC.

In a previous work [20], we identified that increasing the refractive index of the silicon solar cell encapsulant to above 1.59 would drive significant improvement in module efficiency by internal reflection of light reflected from the encapsulated cell surface. The basis of this design guideline was the assumption that the cell texture consisted of {111} faceted upright pyramids. Indeed, when the encapsulant index is above 1.59, normally incident light reflected from the textured surface of the cell at $\theta_r = 38.94°$ is internally reflected at the glass–air boundary. It is clear from the aforementioned measurements of the reflection distribution function that most reflected light is in the range $\theta_r < 35°$, with maxima occurring at yet lower angles. The imperfect nature of the surface texture drives the reflectance to the left on the θ_r scale and, hence, drives the encapsulant refractive index required for total internal reflection well beyond 1.6. Given that encapsulant materials must ideally be transparent across the broadband of wavelengths that make up the solar spectrum, it appears that a suitable high index encapsulant material will be difficult to find. Instead, it should be the goal of silicon solar cell developers to conceive of a surface texturing process yielding higher values of α; in this way, the reflection distribution function would be shifted to higher θ_r, thereby increasing the proportion of reflected light captured by internal reflection at the air–glass interface without placing excessively stringent demands on encapsulant refractive index.

Light trapping and the absorption of infrared light in a silicon solar cell depends on the angle at which light traverses the absorbing silicon substrate. Normally, incident rays pass across a planar substrate following a path perpendicular to its surface. Surface texture extends the ray path by tilting it with respect to the macroscopic surface normal; this is one key way in which the photon absorption capacity of a silicon solar cell can be increased. The length of this path is shortened as α is reduced. For $\alpha = 54.74°$, the path length is $1.33w$, where w is the wafer thickness. Decreasing α to 50° results in a path length of $1.26w$, resulting in a single pass absorptance reduction of 1000-nm radiation ranging between 2% (for $w = 200\,\mu m$) and 5% (for $w = 20\,\mu m$). Employing the Basore model for generation [32] with the light trapping parameters used in [34] and assuming equivalent front surface transmittance, the reduction in α from 54.74° to 50° accounts for a 0.1% ($w = 200\,\mu m$) or 0.2% ($w = 20\,\mu m$) reduction in photogenerated current. By ignoring any impacts on internal reflectance, it is apparent that 'imperfections' in texture morphologies of the magnitude observed in this work have negligible impact on light trapping performance.

5. CONCLUSIONS

We presented an experimental apparatus and methodology suited to the measurement of reflection distributions from textured silicon solar cell surfaces. The technique was validated with a sample having a known surface texture, namely a regular array of inverted {111} faceted pyramids. Reflection distributions measured for 'random pyramid' textured silicon suggest that (i) feature base angles are nearer 50–52° (rather than the commonly assumed value of 54.74°); (ii) a range of base angles is typical; and (iii) typical features are hillocks, rather than {111} faceted upright pyramids.

The standard description of textured surfaces suggests that features are square-based pyramids, with {111} facets. Significant deviation from this standard model was suggested by the experimental results; this deviation has numerous implications for silicon solar cell design, characterisation and modelling. Indeed, typical analyses of front surface reflection, light trapping, photogeneration and surface recombination may be compromised by an inaccurate description of the front surface morphology.

Hillock (rather than pyramid) features and features with lower base angles are associated with higher reflectance of normally incident light. The relative disadvantage of textures having such features is reduced via the application of an optimised ARC so that ~0.2% loss in cell photocurrent is incurred when compared with a texture consisting of {111} faceted upright pyramids. The reduction in base angle from 54.74° to 50° results in a 0.1% to 0.2% reduction in photocurrent because of poorer light trapping.

Finally, we note that the reflection of normally incident light from surfaces with random texture occurs predominantly in the $\theta_r = 20°$ to 30° range—as a result, one can expect virtually no trapping of reflected light via total internal reflection at the air–glass interface of the solar cell module. Surface texturing approaches yielding higher base angles would positively impact upon cell and module performance.

ACKNOWLEDGEMENTS

The authors would like to thank M. A. Green from the University of New South Wales for the productive discussion on texture and its characterisation.

REFERENCES

1. Singh PK, Kumar R, Lal M, Singh SN, Das BK. Effectiveness of anisotropic etching of silicon in aqueous alkaline solutions. *Solar Energy Materials and Solar Cells* 2001; **70**(1): 103–113.
2. Vazsonyi E, De Clercq K, Einhaus R, Van Kerschaver E, Said K, Poortmans J, Szlufcik J, Nijs J. Improved anisotropic etching process for industrial texturing of

silicon solar cells. *Solar Energy Materials and Solar Cells* 1999; **57**(2): 179–188.
3. Nishimoto Y, Namba K. Investigation of texturisation for crystalline silicon solar cells with sodium carbonate solutions. *Solar Energy Materials and Solar Cells* 2000; **61**(4): 393–402.
4. Melnyk I, Wefringhaus E, McCann M, Hefricht A, Hauser A, Fath P. Na_2CO_3 as an alternative to \NaOH/IPA for texturization of monocrystalline silicon. *Proceedings of the 19th European Photovoltaic Solar Energy Conference*, Paris, 2004; 1090–1093.
5. Marrero N, Gonzalez-Diaz B, Guerrero-Lemus R, Borchert D, Hernandez-Rodriguez C. Optimization of sodium carbonate texturization on large-area crystalline silicon solar cells. *Solar Energy Materials and Solar Cells* 2007; **91**(20): 1943–1947.
6. King DL, Buck ME. Experimental optimization of an anisotropic etching process for random texturization of silicon solar cells. *Proceedings of the 22nd IEEE Photovoltaic Specialists Conference*, Las Vegas, 1991
7. You JS, Kim D, Huh JY, Park HJ, Pak JJ, Kang CS. Experiments on anisotropic etching of Si in TMAH. *Proceedings of the 11th International Photovoltaic Science and Engineering Conference*, Hokkaido, 1999; 981–984.
8. Papet P, Nichiporuk O, Kaminski A, Rozier Y, Kraiem J, Lelievre, JF, Chaumartin A, Fave A, Lemiti M. Pyramidal texturing of silicon solar cell with TMAH chemical anisotropic etching. *Solar Energy Materials and Solar Cells* 2006; **90**(15): 2319–2328.
9. Ximello N, Dastgheib-Shirazi A, Scholz S, Hahn G. Influence of pyramid size of chemically textured silicon wafers on the characteristics of industrial solar cells. *Proceedings of the 25th European Photovoltaic Solar Energy Conference*, Valencia, 2010; 1761–1764.
10. Tan S-S, Reed M, Han H, Boudreau R. Morphology of etch hillock defects created during anisotropic etching of silicon. *Journal of Micromechanics and Microengineering* 1994; **4**: 147–155.
11. Bhatnagar YK, Nathan A. On pyramidal protrusions in anisotropic etching of <100> silicon. *Sensors and Actuators A* 1993; **36**: 233–240.
12. Landsberger LM, Naseh S, Kahrizi M, Paranjape M. On hillocks generated during anisotropic etching of Si in TMAH. *Journal of Microelectromechanical Systems* 1996; **5**(2): 106–116.
13. Thong JTL, Luo P, Choi WK, Tan SC. Evolution of hillocks during silicon etching in TMAH. *Journal of Micromechanics and Microengineering* 2001; **11**: 61–69.
14. Zubel I, Kramkowska M. Development of etch hillocks on different Si(hkl) planes in silicon anisotropic etching. *Surface Science* 2008; **602**: 1712–1721.
15. Fornies E, Zaldo C, Albella JM. Control of random texture of monocrystalline silicon cells by angle-resolved optical reflectance. *Solar Energy Materials and Solar Cells* 2005; **87**(1–4): 583–593.
16. Mackel H, Cambre DM, Zaldo C, Albella JM, Sanchez S, Vazquez C, Sanchez I, Vazquez MA. Characterisation of monocrystalline silicon texture using optical reflectance patterns. *Proceedings of the 23rd European Photovoltaic Solar Energy Conference*, Valencia, 2008; 1160–1163.
17. Parretta A. Camera for recording light backscattered from textured photovoltaic samples. *Journal of Optics A: Pure and Applied Optics* 2003; **5**: S284–S292.
18. Parretta A, Bobeico E, Lancellotti L, Morvillo P, Wang A, Zhao J. A new approach to the analysis of light collected by textured silicon surfaces. *Proceedings of the 3rd World Conference on Photovoltaic Energy Conversion*, Osaka, 2003; 122–125.
19. Foldyna M, Moreno M, Roca i Cabarrocas P, De Martino A. Scattered light measurements on textured crystalline silicon substrates using an angle-resolved Mueller matrix polarimeter. *Applied Optics* 2010; **49**(3): 505–512.
20. Baker-Finch SC, McIntosh KR. Reflection of normally incident light from silicon solar cells with pyramidal texture. *Progress in Photovoltaics: Research and Applications* 2011; **19**: 406–416.
21. Van Nijnatten PA. Optical analysis of coatings by variable angle spectrophotometry. *Thin Solid Films* 2008; **516**: 4553–4557.
22. Van Nijnatten PA. An automated directional reflectance/transmittance analyser for coating analysis. *Thin Solid Films* 2003; **442**: 74–79.
23. Green MA. Analytical expressions for spectral composition of band photoluminescence from silicon wafers and bricks. *Applied Physics Letters* 2011; **99**: 131112.
24. Price JB. Anisotropic etching of silicon with KOH-H_2O-Isopropyl Alcohol. *Semiconductor Silicon 1973, eds. HR Huff and RR Burgess (The Electrochemical Society, Princeton NJ)* 1973; 339–353.
25. Merlos A, Acero M, Bao MH, Bausells J, Esteve J. TMAH/IPA anisotropic etching characteristics. *Sensors and Actuators A* 1993; **37–38**: 737–743.
26. Sekimua M. Anisotropic etching of surfactant-added TMAH solution. *Proceedings of the 12th IEEE International Conference on Micro Electro Mechanical Systems*, Orlando, 1999: 650–655.
27. Wind RA, Hines MA. Macroscopic etch anisotropies and microscopic reaction mechanisms: a micromachined structure for the rapid assay of etchant anisotropy. *Surface Science* 2000; **460**: 21–38
28. Campbell PA, Green MA. Light trapping properties of pyramidally textured surfaces. *Journal of Applied Physics* 1987; **62**(1): 243–249.

29. Wefringhaus E, Kesnar C, Lohmann M. Statistical approach to the description of random pyramid surfaces using 3D surface profiles. *Energy Procedia* 2011; **8**: 135–140.
30. Chiao S-C, Zhou J-L, Macleod HA. Optimized design of an antireflection coating for textured silicon solar cells. *Applied Optics* 1993; **32**(28): 5557–5560.
31. Basore PA. Numerical modelling of textured silicon solar cells using PC-1D. *IEEE Transactions on Electron Devices* 1990; **37**(2): 337–343.
32. Basore PA. Extended spectral analysis of internal quantum efficiency. *Proceedings of the 23rd IEEE Photovoltaics Specialists Conference*, 1993; 147–152.
33. Brendel R, Hirsch M, Plieninger R, Werner JH. Wuantum efficiency analysis of thin-layer silicon solar cells with back surface fields and optical confinement. *IEEE Transactions on Electron Devices* 1996; **43**(7): 1104–1113.
34. Baker-Finch SC, McIntosh KR. One-dimensional photogeneration profiles in silicon solar cells with pyramidal texture. *Progress in Photovoltaics: Research and Applications* 2011. DOI: 10.1002/pip.1109.
35. Cousins PJ, Cotter JE. Minimizing lifetime degradation associated with thermal oxidation of upright randomly textured silicon surfaces. *Solar Energy Materials and Solar Cells* 2006; **2**(90): 228–240.
36. Chen FW, Li T-TA, Cotter JE. PECVD silicon nitride surface passivation for high-efficiency n-type silicon solar cells. *Proceedings of the 4th World Conference on Photovoltaic Energy Conversion*, 2006; 1020–1023.
37. McIntosh KR, Johnson LP. Recombination at textured silicon surfaces passivated with silicon dioxide. *Journal of Applied Physics* 2009; **105**: 124520.
38. Gong C, Simoen E, Posthuma NE, Van Kerschaver E, Poortmans J, Mertens R. Study of silicon-silicon nitride interface properties on planar (100), planar (111) and textured surfaces using deep-level transient spectroscopy. *Journal of Physics D: Applied Phyics* 2010; **43**: 485301-1-6.
39. Baker-Finch SC, McIntosh KR. The contribution of planes, vertices and edges to recombination at pyramidally textured surfaces. *IEEE Journal of Photovoltaics* 2011. DOI: 10.1109/jphotov.2011.2165530.